

Microphase Separation, Stress Relaxation, and Creep Behavior of Polyurethane Nanocomposites

Hesheng Xia,¹ Mo Song,¹ Zhongyi Zhang,² Mel Richardson²

¹*Institute of Polymer Technology and Materials Engineering, Loughborough University, Loughborough, Leicestershire LE11 3TU, United Kingdom*

²*Department of Mechanical and Design Engineering, University of Portsmouth, Portsmouth, Hampshire PO1 3DJ, United Kingdom*

Received 7 July 2006; accepted 10 August 2006

DOI 10.1002/app.25462

Published online in Wiley InterScience (www.interscience.wiley.com).

ABSTRACT: The stress relaxation and creep behavior of blank polyurethane (PU) and PU/clay nanocomposites were investigated. The relaxation time spectrum and retardant time spectrum were derived according to the generalized Maxwell model and Voigt model with a Tikhonov regularization method, respectively. The characteristic relaxation time was identified with the corresponding relaxation process. At a small strain, the relaxation was mainly attributed to uncoiling/disentangling of soft segment chain network in the soft phase, with a single characteristic relaxation time in the range of 5–100 s. The increase in the hard segment content leads to a decrease in the relaxation time, and the addition of clay leads to an increase in the relaxation time. At large strains, the multi-

peak relaxations occurred, and they were attributed to the breakup of interconnected hard domains and pullout of soft segment chains from hard domains, together with the disentangling of soft segment chain network in the soft phase. The creep results are consistent with those of the stress relaxation. The relaxation and creep behavior were related to microphase separation of PU. This study suggested that the relaxation spectrum can be used to examine the complicated relaxation processes for a multiphase and multicomponent polymer system. © 2006 Wiley Periodicals, Inc. *J Appl Polym Sci* 103: 2992–3002, 2007

Key words: microphase separation; polyurethane; nanocomposite; stress relaxation; creep

INTRODUCTION

Polyurethane (PU)/clay nanocomposite has attracted increasing interest recently.^{1–11} The introduction of clay can improve tensile strength and elongation of PU. The properties of PU/clay nanocomposites are dependent on the molecular structure of PU, mainly on microdomain structure, dispersion state of clay, i.e., intercalation or exfoliation, and interaction between clay and PU. One of the most important features of PU is microphase separation due to its thermodynamic incompatibility between the soft and hard segments.¹² Microphase separation leads to the formation of two-phase structure, i.e., hard domains rich in hard segments and a soft phase rich in soft segments. The degree of microphase separation influences the mechanical and viscoelastic properties of PU. To disclose the fundamental mechanism about the improvement in PU/nanocomposite properties, the effect of clay on microphase separation of PU has been investigated by several researchers; it appears that there is no consensus. Tien and Wei reported that the degree of microphase separation in

the hard segments of the synthesized montmorillonite (MMT)/PU nanocomposites decreased with the increasing amount of MMT, but reached plateau values at 5 wt % MMT concentration.⁴ Dai et al. found that the degree of microphase separation (i.e., hydrogen bonding index) first increased with the clay ratios in the PU matrix and then decreased.¹¹

PU/clay nanocomposites are viscoelastic, and as a consequence, the long-term strength is one of their major concerns. Stress relaxation and creep were widely used to investigate the time-dependent viscoelastic properties of polymer. Relaxation is a process of reorganization of the structure to reach the thermodynamic equilibrium after a perturbation. It involves the structure change at different length scales, and the required time called relaxation time is on a wide range of time scales. In general, the combination of mechanical elements, usually springs and dashpots, can be used to model the viscoelastic response of polymer materials. It is well known that Maxwell and Voigt model were widely used to depict the stress relaxation and creep behavior, respectively.¹³ The relaxation time spectrum and retardant time spectrum related to specific molecular architectures can be derived from the two models. The spectrum's sensitivity to small changes in molecular connectivity makes it a powerful tool to distinguish small differences in

Correspondence to: M. Song (M.Song@lboro.ac.uk).

otherwise undistinguished materials.¹⁴ For a heterogeneous material, the spectrum is strongly related to the microdomain structure. Relaxation or retardant time spectrum can qualitatively disclose the relationship between the microstructure and characteristic relaxation time. Also, the broadness of the spectrum can reflect the polydispersity of the relaxation elements. For PU with two-phase structure, relaxation or retardant time spectrum can distinguish some information of hard domain and soft phase structures of PU based on the characteristic relaxation peak.

It is interesting to know how the addition of clay affects the microphase separation of PU and further the stress relaxation and creep behavior of PU/clay nanocomposites. In this study, we tried to identify the relaxation peak in the relaxation spectrum and disclose some relationships between microphase separation and stress relaxation and creep behavior in PU/clay nanocomposites.

EXPERIMENTAL

Materials

Poly(propylene glycol) (Lupranol 2090, molecular weight = 6000, function = 3), was kindly provided by Elastogran U.K. Ltd. 4,4'-Methylene bis(cyclohexyl isocyanate) (MDI) was kindly provided by Hyperlast, UK. 1,4-Butanediol was purchased from Aldrich Chemical Company. Dabco-33LV as the catalyst was obtained from Air Products and Chemicals (UK). The organoclay C20A was purchased from Southern Clay Products, USA. The modifiers for organoclay C20A is dihydrogenated tallow quaternary ammonium (2M2HT).

Preparation of PU-organoclay nanocomposites

Polyurethane at different hard segment content, i.e., 16, 26, 36, and 46%, was prepared through one-shot process. Polyurethane/organoclay nanocomposites at a hard segment content of 26% were prepared. The -NCO/OH ratio was kept at 1.1:1 for every sample. Typically, 19.4 g of polyol and 0.6 g of clay were blended and stirred for 4 h at 80°C. The polyol/clay mixture was blended with 0.85 g of 1,4-butanediol, 5.96 g of MDI, and 0.03 g of Dabco-33LV as a catalyst at room temperature for 1 min and was vacuum-degassed for 3–5 min to remove the bubbles. Then the viscous prepolymer was poured into an O-ring metal mold and cured at 50°C for 24 h and 80°C for 72 h to obtain PU-organoclay nanocomposites.

Characterization

Fourier transform infrared (FTIR) spectra of PU/clay nanocomposite films were recorded on a Mattson

3000 FTIR spectrometer by using an ATR mode. The spectra were collected from 4000 to 400 cm⁻¹, with a 4-cm⁻¹ resolution over 120 scans.

Small-angle X-ray scattering (SAXS) experiments were illustrated in reference.¹⁰ It was carried out on the Kratky Compact Small Angle System with a stationary-anode copper-target X-ray tube (wavelength, 1.542 Å) at room temperature. The fine-focus X-ray generator was operated at 45 kV and 40 mA.

The morphology of the samples was examined on sectioned specimens by atomic force microscopy (AFM) using a TA Instruments 2990 micro-thermal analyzer incorporating a ThermoMicroscopes Explorer AFM (TA Instruments, New Castle, DE 19720). The operating method employed was tapping mode, simultaneously producing topographic and phase images. The PU samples were subjected to an initial 50 μm × 50 μm-scan to identify areas smooth enough for analysis. Once this was achieved, a high-resolution 10 μm × 10-μm scan was carried out.

Stress relaxation

Experiment

Stress relaxation tests for the specimens (width, 3.72 mm; thickness, 1–2 mm; length, 35 mm) were carried out using a Hounsfield test machine at room temperature. For strain experiment, the same specimen was used. The specimen was deformed, then relaxed, and then deformed again at a higher strain, following this sequence: 10, 25, 50, 100, 200%. During the test, the specimens were stretched to a certain strain at a crosshead rate of 50 mm/min, and then held for 40 min. For stress relaxation on different hard segment and clay content, different specimens were used for every test, and the strain was fixed at 100%. The stress decay with the time was recorded. The relaxation ratio was defined as $(\sigma_0 - \sigma_e)/\sigma_0$, where σ_0 is the initial stress at $t = 0$ at 100% strain, and σ_e is the approximately equilibrium stress at $t = 40$ min.

Stress relaxation data analysis

Relaxation time spectrum. In general, discrete relaxation time spectrum can be calculated from the experimental relaxation curves using the generalized Maxwell model consisting of a set of Maxwell units connected in parallel. When the number of Maxwell elements approaches infinity, the relaxation modulus can be expressed as Laplace transform of a continuous relaxation time spectrum $H(\tau)$ ¹³.

$$E(t) = E_e + \int_{-\infty}^{\infty} H(\tau) e^{-t/\tau} d \ln \tau \quad (1)$$

where $E(t)$ is the decaying modulus at the time t , τ is the relaxation time, and E_e represents the fitted

equilibrium or residual modulus at the fully decayed state. $H(\tau)$ is the relaxation time spectrum. The spectrum $H(\tau)$ cannot be measured directly. It can be obtained through inverse Laplace transform by a numerical method. The numerical inverse Laplace transform on an experimental curve was generally an ill-posed problem. In this article the relaxation time spectra for all the samples were obtained from the curves of relaxation modulus with time by nonlinear Tikhonov regularization method.¹⁵ A total of 178 data points were selected for the analysis.

Stress relaxation rate. The stress relaxation rate at $t = t_0$ can be estimated by the following equation:

$$\left. \frac{dE(t)}{dt} \right|_{t=t_0} = \left. \frac{d \int_0^\infty \frac{H(\tau)}{\tau} \exp(-t/\tau) d\tau}{dt} \right|_{t=t_0} = \int_0^\infty \frac{H(\tau) \exp(-t_0/\tau)}{\tau^2} d\tau \quad (2)$$

To avoid the initial experimental instability, we calculated the stress relaxation rate at $t = 60$ s. In a previous study, Cotton and Boonstra evaluated the relaxation rate by fitting the test data to an empirical formula, i.e., $f_t = f_{1.0} t^{-n}$, where, $f_{1.0}$ is the stress after 1 min of relaxation, n is the relaxation rate index of material, and t is time in minutes.¹⁶

Creep

Experiment

Creep test for the specimens (width, 4 mm; thickness, 1–2 mm; length, 40 mm) was performed at 30°C on a TA Instruments Thermal Analysis DMA Q800. A small preload of 0.2 N was applied to make sure that the sample was taut. The samples were displaced at a stress of 0.2 MPa for 120 min and then were recovered for 60 min. The strain and creep compliance $J(t)$ was recorded. The creep ratio was defined as $(J_e - J_0)/J_0$, where J_0 is the initial creep compliance, and J_e is the equilibrium creep compliance.

Creep data analysis

Retardant time spectrum. The retardant time spectra were derived according to the generalized Voigt model based on the creep-compliance-time curves.¹³

$$J(t) = J_g + \int_{-\infty}^{\infty} L(\lambda)(1 - e^{-t/\lambda}) d \ln \lambda + t/\eta_0 \quad (3)$$

where $J(t)$ is the creep compliance at the time t , λ is the retardant time, and J_g represents the fitted equilibrium creep compliance. $L(\lambda)$ is the retardant time spectrum.

Creep rate. The creep rate at $t = t_0$ can be estimated by the following equation:

$$\left. \frac{dJ(t)}{dt} \right|_{t=t_0} = \left. \frac{d \int_0^\infty \frac{L(\lambda)}{\lambda} (1 - \exp(-t/\lambda)) d\lambda}{dt} \right|_{t=t_0} = \int_0^\infty \frac{L(\lambda) \exp(-t_0/\lambda)}{\lambda^2} d\lambda \quad (4)$$

To avoid the initial experimental instability, the creep rates at $t_0 = 60$ s were calculated for a relative comparison.

RESULTS AND DISCUSSION

In a multiphase system, microphase separation, i.e., microdomain composition and morphology, has a great influence on the relaxation and creep processes. In this study we first investigate the microphase separation with FTIR, SAXS, and AFM, and then the stress relaxation and creep behavior. We will analyze the stress relaxation and creep behavior combined with the microphase separation of PU.

Microphase separation of polyurethane/clay nanocomposites

FTIR

Phase separation is an important factor for PU physical properties. The degree of phase separation (DPS) in segmented PU can be estimated according to the method of Cooper and coworkers.^{4,17} The hydrogen bonding was formed by the —NH groups being proton donor and the oxygen in carbonyls of the hard segment and in ethers of the soft segment being proton acceptors. The formation of hydrogen bonding by —C=O group can be determined by examining the peak position at $\sim 1705 \text{ cm}^{-1}$ for hydrogen bonded —C=O and at $\sim 1728 \text{ cm}^{-1}$ for free —C=O. By measuring the peak intensity ratio of these two carbonyl groups, it is possible to give an estimate of the degree of hydrogen bonding. In association with the change of absorption peaks of NH groups, the DPS of segmented PU can be calculated. In addition, the hydrogen bonding index, R , can be obtained from a base-line approach method: $R = C_{\text{bonded}}\epsilon_{\text{bonded}}/C_{\text{free}}\epsilon_{\text{free}} = A_{\sim 1703}/A_{\sim 1727}$, where C is the concentration and ϵ is the respective extinction coefficient of bonded and free carbonyl groups. The DPS can be obtained by the equation $\text{DPS} = C_{\text{bonded}}/(C_{\text{bonded}} + C_{\text{free}})$ or $\text{DPS} = R/(R + 1)$.⁴ Here the ratio of $\epsilon_{\text{bonded}}/\epsilon_{\text{free}}$ is taken as ~ 1 according to Cooper and coworkers.¹⁷ Figure 1 shows FTIR spectra of PU/clay composites. The peak was fitted by Microcal Origin software and a curve fitting result for PU-26 is shown inside the Figure 1. The area of

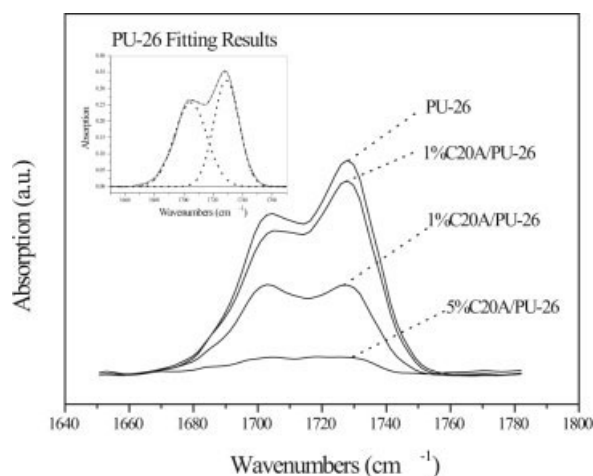


Figure 1 FTIR spectra of PU/clay C20A nanocomposites.

peak at $\sim 1728 \text{ cm}^{-1}$ and $\sim 1705 \text{ cm}^{-1}$ was calculated to evaluate the hydrogen bonding index, R , and the DPS. The DPS results are shown in Figure 2. It is clear that with increasing the clay content, the DPS increased.

AFM

AFM has been proved to be an important tool to characterize the microphase-separated structure.^{18–21} This technique allows simultaneous detection of phase image and height, which provides insight on the variations in topography and local stiffness. Using a tapping mode, AFM can not only image topographic features but can also map the spatial variation in surface by phase imaging. Phase imaging is quite effective for mapping the submicrometer properties of multicomponent polymer systems based on the relative elasticity of individual components. Conventionally, the scales of AFM phase images are set so that the harder phase induces a higher phase offset and appears lighter whereas the softer phase appears darker. Therefore, in the AFM images presented in this article, the lighter regions correspond to the hard phase and clay particles whereas the darker regions are representative of soft phase. In this study the intercalated clay is a minor composition when compared with the hard domain of PU. Figure 3 shows the tapping mode phase images of PU and PU nanocomposite with 3% clay content at a hard segment of 26%. The aggregates of hard domains in the magnitude of submicrometer with the spherical structures were observed in the blank PU. When the clay was incorporated, the size of the aggregates of hard domain was reduced. It is difficult to distinguish the clay particles and hard domain of PU by AFM. The intercalated clay structures were easily observed by TEM, which was shown in our previous study.²² In addition, compared with blank PU, PU nanocomposite has a

clearer interface and a denser hard domain structure, indicating a more complete microphase separation.

So, from FTIR and AFM, it can be concluded that with the addition of clay, the size of hard microdomain decreases and a more complete phase separation occurs. In a previous study,¹⁰ we conducted SAXS experiment to examine the microphase morphology of PU. The degree of microphase separation also can be evaluated from SAXS experimental. The higher electron density variance is due to a higher extent of microphase separation, which leads to a greater contrast in electron densities. The scattering peak height is roughly proportional to the contrast between the phases.^{23,24} The scattering peak height increases by increasing the clay content, indicating a higher degree of microphase separation. The SAXS results are consistent with the results reported here. The reason for the change in microphase separation induced by clay particles is not very clear. Possibly, the clay particles can have the nucleation effect to induce the formation of hard domain during the reaction process.

Stress relaxation of blank polyurethane

Stress relaxation measurements can give an insight into the viscoelastic behavior of polymer. Typical stress relaxation data can be fitted to a power-law equation $E(t) \sim E_{\infty} (1+(t/\tau)^{-m})^{25}$ or a single stretched exponential function $E(t) = (E_0 - E_f) \exp(-t/\tau)^{\beta} + E_f$, a modification of the Kohlrausch–Williams–Watt equation.²⁶ A single characteristic relaxation time τ can be derived. For an elastomer, the stress relaxation with the power-law decay was related to the relaxation of loops and free dangling chains attached to the hard domain.²⁷ Recently, Hotta and colleagues proposed a chain pullout mechanism to interpret the stretched exponential decay.^{28,29} Gurtovenko and Gotlib thought that the stress relaxation behavior in an inhomogeneously crosslinked network may be

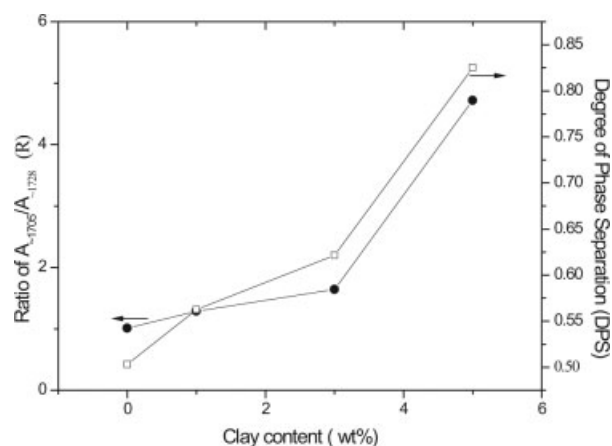


Figure 2 Variation of hydrogen index with the clay content.

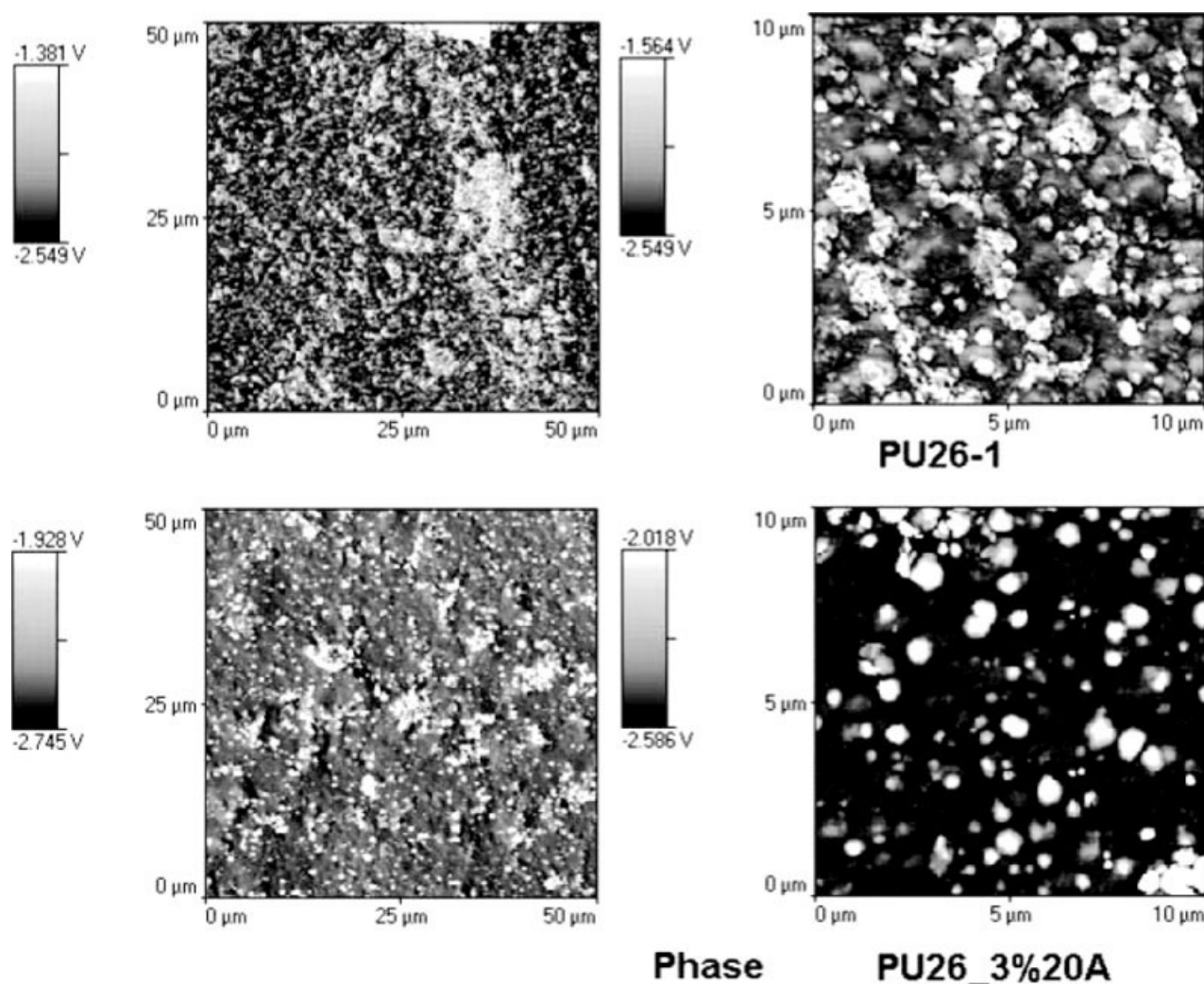


Figure 3 AFM tapping-mode phase image of PU and PU/3% clay C20A nanocomposite.

caused by a broad size distribution of noninteracting network regions each composed of a certain number of relaxation elements (crosslinks, polydisperse chains, etc).³⁰ Hotta extended this model to homogeneously crosslinked thermoplastic elastomers assuming that thermal fluctuations induce fluctuations in size of domains of crosslinks via a chain-pullout mechanism.²⁹ Ortiz et al. studied a single-step stress relaxation of a polydomain liquid crystalline elastomer (LCE); they found that an LCE with a domain structure has a higher relaxation strength and a much faster relaxation time when compared with amorphous, isotropic polyisoprene and they suggested that the origin of this relaxation takes place on a localized size scale of less than a single domain ($\sim \mu\text{m}$).³¹ For a multiphase and multicomponent system, the stress relaxation is a superposition of different relaxation processes. The different relaxation processes with different relaxation elements should be related to different characteristic relaxation times τ . The power-law and stretched exponential equations with a single

relaxation time cannot give such information. Alternatively, the quantitative description of stress relaxation as shown in Eq. (1) can be made according to a gener-

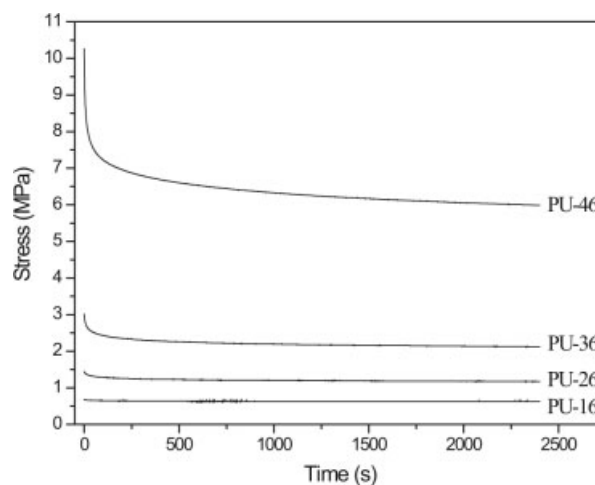


Figure 4 Stress relaxation curves of PU with different hard segment contents at 100% strain.

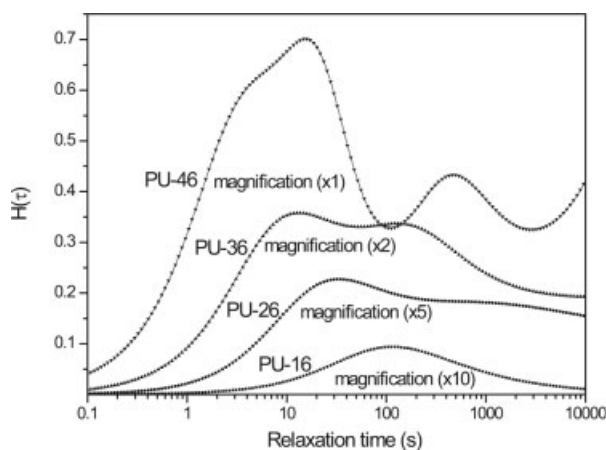


Figure 5 Relaxation time distribution curves of PU with different hard segment contents.

alized Maxwell model based on the stress relaxation modulus data $G(t) = \sigma(t)/\epsilon$. And the relaxation time spectrum $H(\tau)$ can be derived using Laplace transform. The $H(\tau)$ value is related to relaxation rate, as shown in Eq. (2). The multiple characteristic relaxation time and relaxation peak broadness given by relaxation time spectrum $H(\tau)$ can disclose the molecular and microdomain structure information qualitatively. The stress relaxation for polymer is attributed to chain motion and orientation, uncoiling/disentangling of polymer chain network strand, and deformation and rupture of microdomain and crosslinks. Our belief is that every peak in the relaxation time spectrum should be related to a specific intrinsic structural change. In this study, to identify every relaxation peak in relaxation time spectrum, we first examine the hard segment content and strain effect of blank PU.

Hard segment content

Figures 4 and Figure 5 show the stress relaxation curves and relaxation time spectra of PU with different hard segment contents. The initial stress, equilibrium stress, relaxation ratio, relaxation rate, and characteristic relaxation time are listed in Table I. By increasing the hard segment content, the initial stress

and equilibrium stress, relaxation ratio and rate increased. Figure 6 shows the variation of characteristic relaxation time τ with the hard segment content. Based on the relaxation time spectrum, three points can be noted. (1) As shown in Figure 6, the characteristic relaxation time decreased with increasing hard segment content, and this decrease can be fitted to an empirical exponential equation very well: $\tau = 5 + 957 \exp(-c/0.07)$, where c is the hard domain content. Based on this equation, when hard domain content was extrapolated to 0, the PU without hard domain has a relaxation time of ~ 962 s. It is in the same magnitude of isotropic polyisoprene investigated by Ortiz et al.³¹ When the hard domain content was extrapolated to 100%, the pure hard domain has a relaxation time of ~ 5 s. (2) At a 16% hard segment content, there is only one relaxation peak. And by increasing the hard segment content, another peak with a longer relaxation time appeared and became much clearer at 36 and 46% hard segment contents. (3) By increasing the hard segment content, the peak becomes broader. These results suggest that the hard segment content has a significant effect on the relaxation of PU. A detailed discussion will follow later.

Strain effect

The strain plays an important role in the structural change of elastomer during stress relaxation. The strain experiment was conducted at different strains 10, 25, 50, 100, and 200% for blank PU at a 26% hard segment content. Figure 7 shows the relaxation time spectra at different strains. With the increase in strain, the characteristic relaxation time first decreased and then increased and it appears that the relaxation peak first becomes narrower and then broader. At a strain of 200%, three characteristic peaks appeared. The multippeak distribution at this large strain indicates a multirelaxation process.

From the above-mentioned relaxation experiments by varying the hard segment and strain, we attempt to identify the peak related to the relaxation process. For PU elastomer, there should be three main relaxa-

TABLE I
Stress Relaxation Data of Unfilled Polyurethane at Different Hard Segment Contents

Sample	Initial stress σ_0 (MPa)	Equilibrium stress σ_e (MPa)	Relaxation ratio $(\sigma_0 - \sigma_e)/\sigma_0$	Relaxation rate at 60 s (10^{-4})	Relaxation time τ (s)
PU-16	0.67	0.63	0.050	1.22	116.6
PU-26	1.44	1.17	0.188	6.80	31.9
PU-36	3.01	2.12	0.296	26.8	11.6
PU-46	10.26	5.99	0.416	72.2	7.0

Relaxation rate was obtained from eq. 2, and the characteristic relaxation time τ was taken from the position of the maximum in the short time-relaxation peak. For PU-46, the first wide peak was split into two peaks by using an origin fitting program and the τ value was taken from the first short time-relaxation peak.

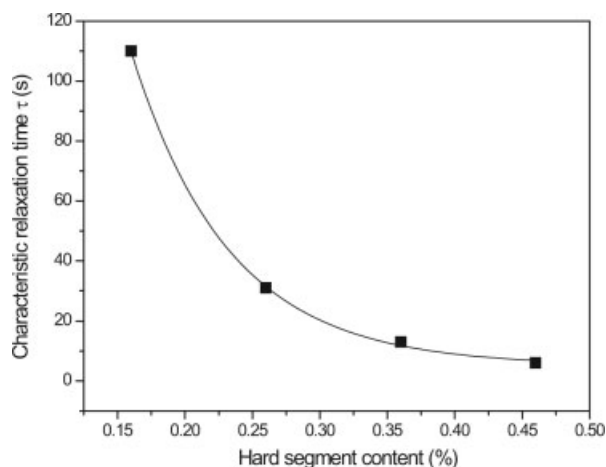


Figure 6 Variation of characteristic relaxation time with different hard segment contents.

tion processes: uncoiling/disentangling of soft segment chain network in the soft phase, breakup of interconnected hard domain, and pullout of soft segment chains from hard domains. The first relaxation can take place at any strain, and the latter two relaxations only at large strains. One of our main concerns is, What mechanism is responsible for the relaxation process with the characteristic peak at 5–100 s? We think this peak should be attributed to uncoiling/disentangling of soft segment chain network in the soft phase. There are two reasons for this identification: (1) as suggested earlier, from the strain experiment this peak always existed at a small strain (linear viscoelastic region) and large strains (nonlinear viscoelastic region). The strain experiment was conducted on one elastomer specimen following this sequence: 10, 25, 50, 100, 200%. Even after several relaxation experiments, the characteristic relaxation peak at 5–100 s still existed with some shifts, suggesting that the related relaxation process may be reversible. (2) From relaxation experiment with different hard segment contents, the peak shifts to a larger relaxation time with the increase of soft segment content. If we attribute this peak to the structural change of hard domain, there should be another peak for soft segment chain for PU-16; however, it is clear that there is only one single peak. The peak shift with increasing soft segment content should be related to soft phase composition, i.e., the hard segment content in the soft phase. With the increase in hard segment content, the hard segment in the soft phase increased, soft chain flexibility decreased (glass transition temperature increase), and elasticity decreased, thus leading to a fast stress relaxation time. For PU relaxation at a large strain of 200%, the observed three peaks in the relaxation spectrum (Fig. 7) was attributed to three different processes. The first peak I at ~ 6 s may be attributed to the breakup of interconnected hard domains, the second peak II at ~ 47 s

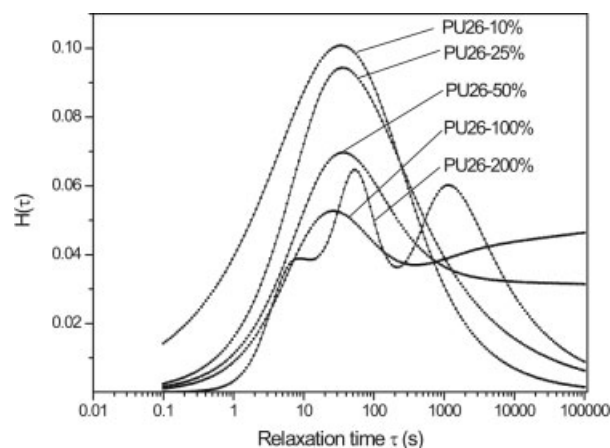


Figure 7 Effect of strain on the relaxation spectrum of blank PU.

should be attributed to the disentanglement of the molecular chains in the soft domain, and the third peak III at ~ 1443 s may be attributed to the pullout of soft segment chains from hard domains, which takes place after the breakup of interconnected hard domain. We believed that the multippeak appeared at a large strain of 200% was related to the breakup of interconnected hard domains. The breakup of interconnected hard domains during stretching was also detected by FTIR based on a decrease in hydrogen-bonding.^{32,33} Ishihara et al. reported strain-induced changes in the extent of hydrogen bonding on one elastomer.³⁴ They suggested that no change in the extent of hydrogen bonding of polyurethaneureas was observed up to 50% strain, and an abrupt decrease in the hydrogen bonding occurred at 100% strain, which was followed by only a slight decrease in H-bonding at still higher elongation. Desper et al.³⁵ reported a significant decrease in a long repeat period at the strain between 100 and 200% by SAXS experiment and deduced the breakup of the

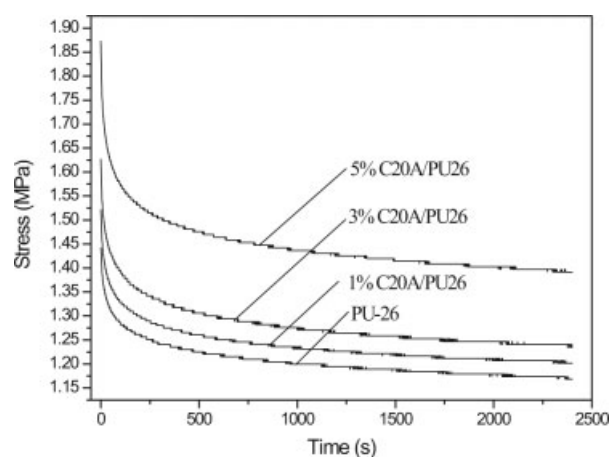


Figure 8 Stress relaxation curves of PU/clay C20A nanocomposites at 100% strain.

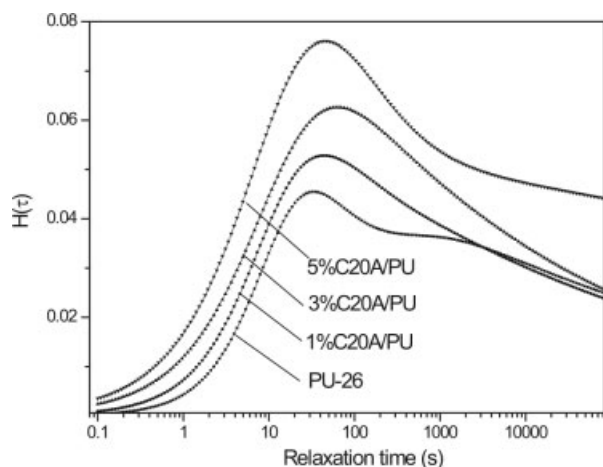


Figure 9 Relaxation time distribution curves of PU/clay C20A nanocomposites.

hard-segment phase into smaller chunks. This present study suggested that the relaxation spectrum $H(\tau)$ can characterize the rupture of interconnected hard domains of PU and give more information on this dynamic process than can FTIR and SAXS. In addition, we noted that with increase in the hard segment content, the relaxation spectra changed from single-peak distribution to multippeak distribution. These results suggested that increasing hard segment content led to a more complicated relaxation process. Especially, the shape of relaxation spectrum of PU with a 46% hard segment content at 100% strain is similar to that of PU with a 26% hard segment content at a 200% strain. In such cases, the breakup of interconnected hard domains of PU occurred and led to the multippeak relaxation. The strain needed to break up the interconnected hard domains of PU at high hard segment contents is lower than that at low hard segment contents. This is because the interconnected hard domains of PU at higher hard segment contents have a larger size and could be more easy to deform and break under strain.

Stress relaxation of polyurethane nanocomposite

We have identified the relaxation peak based on the relaxation experiment of PU at different hard seg-

ment contents and different strains. We will discuss the effect of clay on the relaxation time of PU nanocomposites, mainly the characteristic relaxation time at 5–100 s related to uncoiling/disentangling of soft segment chain network in the soft phase.

Effect of clay content on stress relaxation

Figures 8 and Figure 9 show the stress relaxation curves and relaxation time spectra for PU with different clay contents, respectively. The initial stress, equilibrium stress, relaxation ratio, relaxation rate, relaxation time are listed in Table II. With the increase in clay content, the initial stress increased and the equilibrium stress nearly does not change except for 5% C20A. The addition of clay can improve the modulus of PU elastomer, which is consistent with our former conclusion.^{7,22} The results indicate that the addition of clay has a very weak effect on the crosslink density of PU. The relaxation ratio and rate increase with the addition of clay. It is interesting to note that the characteristic relaxation time related to uncoiling/disentangling of soft segment chain network in the soft phase increased with the addition of clay. This suggested that characteristic relaxation time derived from relaxation spectrum is not always related to the overall relaxation rate, as suggested in eq. 2. The characteristic relaxation time only correlates a specific relaxation process. This is different from relaxation time obtained from the power-law equation or a single stretched exponential function, which can be taken as an evaluation of overall relaxation rate. The peak shift with clay content could be related to soft phase composition. As suggested earlier, the addition of clay enhanced the degree of microphase separation; that means the hard segment content in the soft phase decreased, soft chain flexibility increased, and elasticity increased, thus leading to a slow stress relaxation process. We noted that the trend in the change of microphase separation with clay contents is consistent with the trend in the relaxation time. On the other hand, with the addition of clay, the relaxation peak becomes broader. The broadening of relaxation spectra is associated with

TABLE II
Stress Relaxation Data of Polyurethane/Clay Nanocomposites at 26 wt % Hard Segment Content

Sample	Initial stress σ_0 (MPa)	Equilibrium stress σ_e (MPa)	Relaxation ratio $(\sigma_0 - \sigma_e)/\sigma_0$	Relaxation rate at 60 s (10^{-4})	Relaxation time τ (s)
PU-26	1.44	1.17	0.188	6.80	31.9
1% C20A	1.52	1.20	0.210	8.04	43.1
3% C20A	1.63	1.23	0.241	9.67	61.8
5% C20A	1.87	1.39	0.257	11.50	46.3

Relaxation rate was obtained from eq. 2, and the relaxation time τ was taken from the position of the maximum in the short time-relaxation peak.

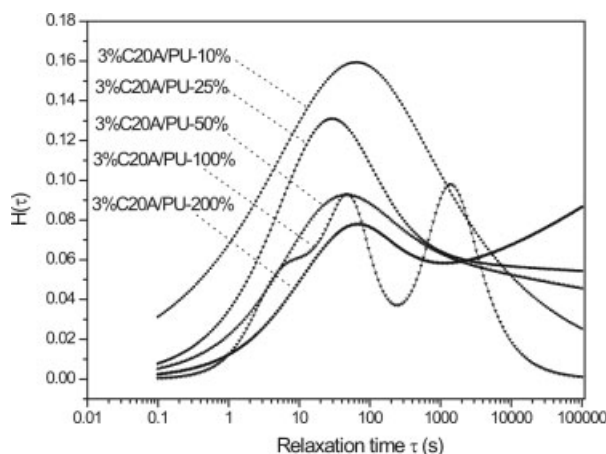


Figure 10 Effect of strain on the relaxation spectrum of PU/3%clay nanocomposite.

the increase in the diversity of soft segment chain structure due to the addition of the filler.

Strain effect

The strain experiments were conducted at different strains 10, 25, 50, 100, and 200% for 3% C20A/PU nanocomposite. Figure 10 shows the relaxation time spectra at different strains. During the test, the specimen was deformed, then relaxed, and then deformed again at a higher strain, following this sequence: 10, 25, 50, 100, 200%. The specimens were stretched to a certain strain at a crosshead rate of 50 mm/min, and then held for 40 min. The characteristic relaxation times of PU nanocomposite at different strains are higher than that of blank PU at the corresponding strain shown in Figure 8. A multippeak distribution appeared at 100% strain for PU/3% C20A nanocomposites, earlier than blank PU, possibly due to a faster overall relaxation rate. At a 200% strain, the relaxation

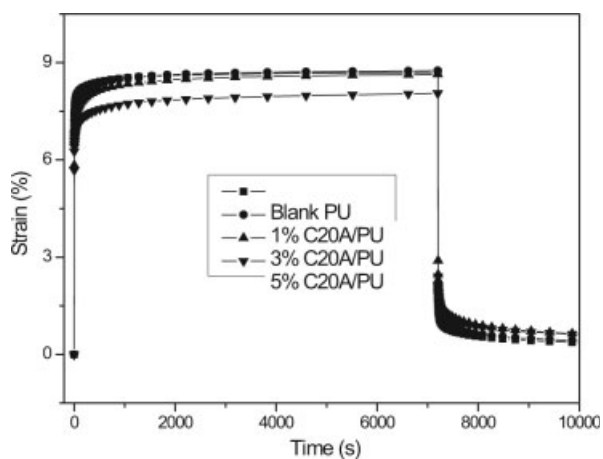


Figure 11 Creep and recovery curves of PU/clay C20A nanocomposites.

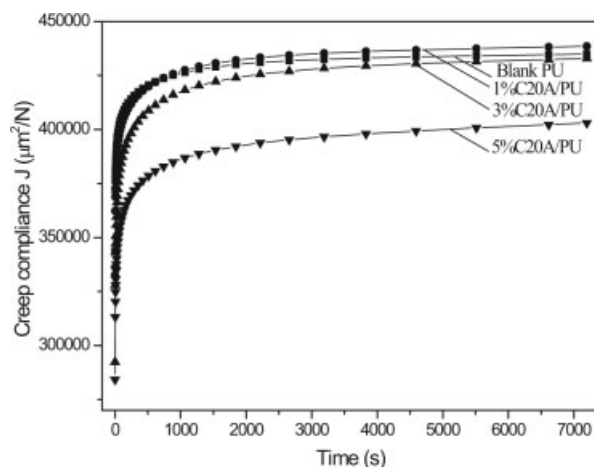


Figure 12 Creep compliance versus time curves of PU/clay C20A nanocomposites.

spectra return to a single peak distribution. This indicated that the two new relaxation processes that appeared at a 100% strain involved an irreversible disruption process. This further supported that it is reasonable to attribute the two processes to the breakup of interconnected hard domains and the pullout of soft chains from hard domains, respectively.

Creep of polyurethane nanocomposites

Creep is defined as the time-dependent permanent deformation in a material resulting from prolonged application of constant structural stress at a constant temperature. For polymer, after instantaneous deformation, the creep can be divided into two main stages: the primary creep and the steady-state creep. In the primary creep, the creep strain rate decreases with time. In the steady-state creep, the strain rate is constant. When load is removed after a creep time,

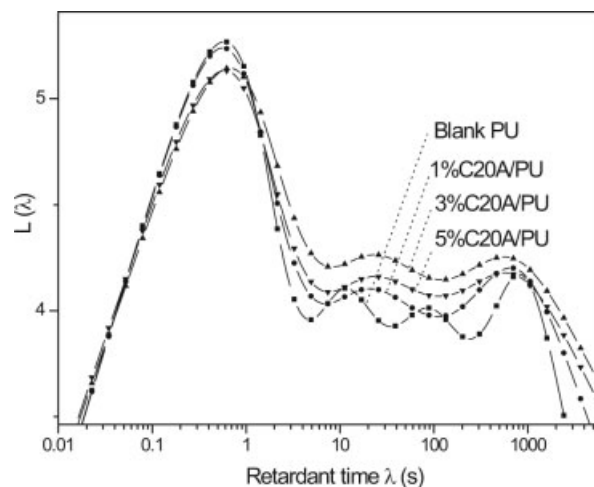


Figure 13 Retardant time distribution curves of PU/clay nanocomposites.

TABLE III
Creep Data of Polyurethane/Clay Nanocomposites at 26 wt % Hard Segment Content

Sample	Instantaneous compliance $J_0(10^5 \mu\text{m}^2/\text{N})$	Equilibrium compliance $J_e(10^5 \mu\text{m}^2/\text{N})$	Creep ratio $(J_e - J_0)/J_0$	Creep rate at 60 s (10^{-2})	Retardant time λ (s)
PU-26	3.438	4.350	0.265	6.74	11.5
1% C20A	3.325	4.384	0.318	6.90	21.4
3% C20A	2.920	4.329	0.483	7.17	24.0
5% C20A	2.840	4.031	0.419	7.02	23.8

The creep rate was obtained from eq. 4, and the retardant time λ was taken from the position of the maximum of the second peak of the retardation spectra.

strain recovery occurs, which means creep recovery. In general, in a creep test the total strain ε is the sum of three separate parts ε_1 , ε_2 , and ε_3 . The ε_1 and ε_2 are the immediate elastic deformation and delayed elastic deformation. ε_3 is the Newtonian flow.¹³ Figure 11 shows the creep and recovery curves of PU/clay C20A nanocomposites. With increase in clay content, the ε_1 and ε_2 decreased. Also, the addition of clay leads to a lower creep recovery. The creep compliance J , i.e., the ratio of strain and applied stress, can be expressed as $J = J_1 + J_2 + J_3$. For a crosslinked or highly crystalline polymers, J_3 can be 0 approximately.¹³ Figure 12 shows the creep compliance curves for PU with different clay contents. The quantitative description of creep can be made according to a generalized Voigt model based on the creep compliance data as shown in Eq. (3). And the retardation spectrum can be derived using Laplace transform. Similar to relaxation time spectrum, the retardant spectrum $L(\lambda)$ value is related to creep rate as shown in Eq. (4). Figure 13 shows the retardant time spectra for PU with different clay contents. The instantaneous compliance, equilibrium compliance, creep ratio, creep rate, and retardant time are listed in Table III. Here, the retardant time λ was taken from the position of the maximum of the second peak of the retardation spectra. We choose this peak because the retardant time obtained from this peak is in the same magnitude as the relaxation time we discussed earlier. With increase in clay content, the instantaneous compliance decreases, which is consistent with the analysis of the relaxation modulus. Also, the equilibrium compliance nearly does not change except for 5% C20A, similar to the equilibrium stress during the stress relaxation experiment. The creep ratio and rate increased and the retardant time increased with the addition of clay. These results agree with the stress relaxation results.

CONCLUSIONS

Microphase separation of PU nanocomposite was characterized. FTIR, AFM, and SAXS suggested that

with the addition of clay, the size of hard domain decreased and a more complete phase separation occurred. Based on the stress relaxation modulus and creep compliance data, the relaxation and retardant time spectra were derived according to a generalized Maxwell model and Voigt model with a Tikhonov regularization method, respectively. Based on stress relaxation of blank PU, the characteristic relaxation peaks in the spectrum were assigned to different relaxation processes. At a strain below 100%, the disentanglement of the molecular chains in the soft domain should be mainly responsible for the stress relaxation process. It was found that relaxation time decreases with increasing hard segment content. The addition of clay increases the relaxation time. The shift in the relaxation time was related to microphase separation of PU. At large strains, the occurred multipeak relaxations were related to the breakup of interconnected hard domains, pullout of soft segment chains from hard domains, and the disentanglement of the molecular chains in the soft phase; the former two processes are irreversible. The relaxation spectrum $H(\tau)$ can be used to characterize the rupture of interconnected hard domain of PU and provide a method to examine the complicated relaxation processes for a multiphase and multicomponent polymer system. In addition, the creep results are in agreement with those of the stress relaxation tests.

References

1. Wang, Z.; Pinnavia, T. J. *Chem Mater* 1998, 10, 3769.
2. Zilg, C.; Thomann, R.; Mulhaupt, R.; Finter, J. *Adv Mater* 1999, 11, 49.
3. Yao, K. J.; Song, M.; Hourston, D. J.; Luo, D. Z. *Polymer* 2002, 3, 1017.
4. Tien, Y. I.; Wei, K. H. *Polymer* 2001, 42, 3213.
5. Tien, Y. I.; Wei, K. H. *Macromolecules* 2001, 34, 9045.
6. Osman, M. A.; Mittal, V.; Morbidelli, M.; Suter, U. W. *Macromolecules* 2003, 36, 9851.
7. Song, M.; Hourston, D. J.; Yao, K. J.; Toly, J. K. H. *J Appl Polym Sci* 2003, 90, 3239.
8. Rhoney, I.; Brown, S.; Hudson, N. E.; Pethrick, R. A. *J Appl Polym Sci* 2004, 91, 1335.
9. SolarSKI, S.; Benali, S.; Rochery, M.; Devaux, E.; Alexandre, M.; Monteverde, F.; Dubois, P. *J Appl Polym Sci* 2005, 95, 238.

10. Song, M.; Xia, H. S.; Yao, K. J.; Hourston, D. J. *Eur Polym J* 2005, 41, 259.
11. Dai, X. H.; Xu, J.; Guo, X. L.; Lu, Y. L.; Shen, D. Y.; Zhao, N.; Luo, X. D.; Zhang, X. L. *Macromolecules* 2004, 37, 5615.
12. Hepburn, C. *Polyurethane Elastomer*; Applied Science Publishers: London, 1982.
13. Ferry, J. D. *Viscoelastic Properties of Polymers*, 3rd ed.; Wiley: New York, 1980.
14. Mours, M.; Winter, H. H. In *Experimental Methods in Polymer Science: Modern Methods in Polymer Research and Technology*; Tanaka, T., Ed.; Academic Press: San Diego, CA, 2000; pp 495-546, .
15. Honerkamp, J.; Weese, J. *Rheol Acta* 1993, 32, 57.
16. Cotton, G. R.; Boonstra, B. B. *J Appl Polym Sci* 1965, 9, 3395.
17. Seymour, R. W.; Ester, G. M.; Cooper, S. L. *Macromolecules* 1970, 3, 579.
18. Granddy, D. B.; Hourston, D. J.; Price, D. M.; Reading, M.; Silva, G. G.; Song, M.; Sykes, P. A. *Macromolecules* 2000, 33, 9348.
19. Eaton, P. J.; Estarlich, F. F.; Ewen, R. J.; Nevell, T. G.; Smith, J. R.; Tsibouklis, J. *Langmuir* 2002, 18, 10011.
20. Eaton, P. J.; Graham, P.; Smith, J. R.; Smart, J. D.; Nevell, T. G.; Tsibouklis, J. *Langmuir* 2000, 16, 7887.
21. Garrett, J. T.; Siedlechi, C. A.; Runt, J. *Macromolecules* 2001, 34, 7066.
22. Xia, H. S.; Shaw, S. J.; Song, M. *Polym Int* 2005, 54, 1392.
23. Saiani, A.; Rochas, C.; Eeckhaut, G.; Daunch, W. A.; Leenslag, J.-W.; Higgins, J. S. *Macromolecules* 2004, 37, 1411.
24. Li, W.; Ryan, A. J.; Meier, I. K. *Macromolecules* 2002, 35, 5034.
25. Chasset, R.; Thirion, P. In *Proceedings of the Conference on Physics of Non-Crystalline Solid*; Prins, J. A., Ed.; North-Holland: Amsterdam, 1965; p 345.
26. Williams, G.; Watts, D. C. *Trans Faraday Soc* 1971, 67, 1323.
27. Curro, J. G.; Pincus, P. *Macromolecules* 1983, 16, 559.
28. Hotta, A.; Clarke, S. M.; Terentjev, E. M. *Macromolecules* 2002, 35, 271.
29. Baeurle, S. A.; Hotta, A.; Gusev, A. A. *Polymer* 2005, 46, 4344.
30. Gurtovenko, A. A.; Gotlib, Y. Y. *J Chem Phys* 2001, 115, 6785.
31. Ortiz, C.; Ober, C. K.; Kramer, E. J. *Polymer* 1998, 39, 3713.
32. Wang, C. B.; Cooper, S. L. *Macromolecules* 1983, 16, 775.
33. Seymour, R. W.; Allegranza, A. E.; Cooper, S. L. *Macromolecules* 1973, 6, 896.
34. Ishihara, H.; Kimura, I.; Saito, K.; Ono, H. *J Macromol Sci Phys* 1974, 10, 591.
35. Desper, C. R.; Schneider, N. S.; Jasinski, J. P.; Lin, J. S. *Macromolecules* 1985, 18, 2755.